HADLEY CENTRE TECHNICAL NOTE NO. 14

THE INDIRECT EFFECTS OF ANTHROPOGENIC SULPHATE AEROSOL SIMULATED USING A CLIMATE MODEL WITH AN INTERACTIVE SULPHUR CYCLE

By

A Jones, D L Roberts and M J Woodage

December 1999

Hadley Centre for Climate Prediction and Research
Meteorological Office
London Road
Bracknell
Berkshire RG12 2SY

NOTE: This paper has not been published. Permission to quote from it should be obtained from the Director of the Hadley Centre.

Abstract

The effects of anthropogenic sulphate aerosols on cloud albedo and on precipitation efficiency (the first and second indirect effects respectively) are investigated using a version of the Hadley Centre climate model. This version includes a new cloud microphysics scheme, an interactive sulphur cycle and a parametrization of the effects of sea-salt aerosols. The combined global mean radiative impact from both indirect effects is estimated to be approximately -1.0 Wm^{-2} in terms of the change in net radiation at the top of the atmosphere; this is found to be less than the cumulative impact of each effect considered separately. This estimate of the total effect has at least a factor of 2 uncertainty associated with it: for example, neglecting sea-salt aerosol leads to a 27% increase in the radiative impact of anthropogenic sulphate, and different autoconversion parametrizations lead to differences in the second indirect effect of a factor of three.

1 Introduction

The impact of anthropogenic sulphate aerosols on the Earth's radiation budget may be divided into direct and indirect effects. The former involves the direct scattering or absorption of incoming solar radiation by the aerosol particles. The latter concerns the effects of aerosol particles on the radiative properties of clouds. The direct effect has been estimated to exert a negative (cooling) radiative forcing on the climate system in the range -0.2 to -0.8 Wm^{-2}, which is significant when compared with the estimated positive (warming) forcing of $+2.5$ Wm^{-2} from increases in greenhouse gases to date (all estimates IPCC 1996). The indirect effects of aerosols operate by increasing the number concentration of cloud condensation nuclei (CCN), so increasing the concentration of cloud droplets and thereby (assuming constant cloud water content) reducing the mean size of cloud droplets (Twomey 1974). This reduction in cloud droplet size has two further effects: firstly, clouds with smaller droplets reflect more solar radiation back to space; this first indirect effect is sometimes known as the 'albedo' effect. Previous work has estimated this effect to be in the range -0.5 to -1.5 Wm^{-2} (Boucher & Lohmann 1995, Jones & Slingo 1996). Secondly, the reduction in cloud droplet size also affects the efficiency with which clouds form precipitation, tending to increase the amount of water in clouds and also affecting their persistence. Consequently, this second indirect effect (sometimes known as the 'lifetime' effect), as well as having a cooling effect in the shortwave due to the clouds being brighter, could also exert a longwave warming influence due to the increase in cloud water.

The early stages of cloud droplet growth occur by the condensation of water vapour onto CCN once the relative humidity just exceeds 100%. However, the rate of condensational growth slows as the droplets become larger, and this process alone cannot account for the formation of precipitation-sized particles in warm clouds in the

times observed (Pruppacher & Klett 1997). Precipitation production in non-freezing clouds depends on the runaway growth of a small fraction of cloud droplets which become large enough to fall with appreciable speeds relative to the other cloud droplets, so colliding and coalescing with them and thereby growing larger. The process of precipitation formation by this collision-coalescence mechanism is referred to as the autoconversion of cloud water to rainwater. For the same cloud water content, autoconversion is slower for a higher concentration of smaller droplets than for a lower concentration of larger droplets. This is because smaller droplets have lower relative fallspeeds, tend to flow around one another rather than colliding and coalescing, and also require more collisions to reach raindrop size; this is the basis of the 'lifetime' effect.

Albrecht (1989) proposed that increases in CCN could decrease the formation rate of drizzle in marine stratiform clouds. This would reduce the rate at which the cloud water was dissipated, so increasing the lifetime of the cloud and thereby exerting a cooling effect by the increased persistence of reflective clouds. Experimental studies over the eastern Pacific of the effects of aerosols from ship exhausts on clouds support the validity of this mechanism (Durkee *et al.* 1999; Ferek *et al.* 1999). Over the Atlantic, measurements of clean and polluted clouds have found a relative dearth of drizzle drops in polluted clouds (Hudson & Li 1995). The mechanism is also supported by detailed cloud/boundary-layer models (Ackerman *et al.* 1995). General circulation model (GCM) studies of both indirect effects (Lohmann & Feichter 1997, Rotstayn 1999) have found that the second effect is of a similar magnitude to the first, indicating that account should be taken of it in modelling recent and future climate change.

In this study we use a newly-developed interactive sulphur cycle and a new microphysics scheme to estimate the impact of the first and second indirect effects in the Hadley Centre GCM. In addition to modelling sulphate aerosol, this study also includes a parametrization of the effects of sea-salt aerosol. The climate model and details of modelling the indirect effects are presented in Sections 2 and 3. The sulphur cycle is described in Section 4, and the general design and rationale of the experiments in Section 5. The results are presented in Section 6, and discussion of these results and some conclusions are given in Section 7. Finally, a brief discussion of current and future work is presented in Section 8.

2 The Climate Model

The model used in this study was based on HadAM3 (Pope *et al.* 1999), the atmospheric component of the current climate model configuration of the UK Meteorological Office's Unified Model (Cullen 1993). The model has a resolution of 2.5° latitude by 3.75° longitude with 19 levels in the vertical (defined in Appendix A) and was run with a timestep of 30 minutes and climatological sea-surface temperatures as a

boundary condition. The main improvements since the previous version (Johns *et al.* 1997) include a new radiation scheme (Edwards & Slingo 1996), the inclusion of convective momentum transport (Gregory *et al.* 1997) and a new land surface scheme (Cox *et al.* 1999).

The version of the model used here has been modified to include a new treatment of large-scale (*i.e.* non-convective) clouds and to introduce a new mixed-phase precipitation scheme with explicit microphysics (Wilson & Ballard 1999). The cloud scheme is based on that of Smith (1990), but instead of having only one prognostic variable for total water (vapour + liquid + ice) it has been extended to use two prognostic variables, one for vapour plus cloud liquid and one for cloud ice. The partitioning between liquid- and ice-phase cloud is based on explicit modelling of the relevant microphysical processes. The microphysical exchange terms in the new mixed-phase precipitation scheme are based on Rutledge & Hobbs (1983) but with alterations to the ice/snow fallspeeds (based on Heymsfield 1977) and to the autoconversion of cloud water to rain (see Section 3 below). Full details are given in Wilson & Ballard (1999).

A further modification to HadAM3 in the model used here is the inclusion of a prognostic sulphur-cycle scheme. This allows the model to calculate the distribution of sulphate aerosol mass concentration interactively, as opposed to using fixed time-mean fields of sulphate calculated in separate experiments as employed previously. This new scheme is outlined in Section 4 below.

Cloud droplet effective radii (r_e) can be set to a standard value of 7μm or else can be parametrized. For stratiform and shallow convective clouds (those less than 500m in depth) the parametrization of Martin *et al.* (1994) is used:

$$r_e = (3\,L / 4\pi\,\rho_w\,k\,N_d)^{1/3}. \qquad (1)$$

L is the cloud liquid water content (kg m^{-3}), ρ_w the density of water and N_d is the cloud droplet number concentration, which in the standard scheme is set to 6.0×10^8 m^{-3} over land and 1.5×10^8 m^{-3} over ocean (Bower & Choularton 1992). The value of k depends on whether the clouds are continental or maritime (taken as whether over land or sea in the model) — see Martin *et al.* for details. For deep convective clouds the constant values suggested by Bower & Choularton (1992) are used. The characteristic particle size for ice crystals is calculated using the parametrization of Kristjánsson *et al.* (1999). This parametrization depends only on temperature and so there is no contribution from the ice-phase to the indirect effects modelled here. Below 0°C clouds are separated into adjacent liquid and ice regions for radiative purposes, the relative sizes of the regions depending on the cloud liquid- and ice-water contents.

Experiments concerning the indirect effects of aerosols require that the fixed values of N_d used as standard are replaced by values determined from aerosol concentrations. In the model used here the cloud droplet number concentration depends on three factors:

2.1 Sulphate

Although it is now well established that sulphate does not dominate aerosol composition as much as once thought (*e.g.* Rivera-Carpio *et al.* 1996, Hegg *et al.* 1997, Murphy *et al.* 1998), it is nevertheless still an important component of the atmospheric aerosol. In the model the number concentration of sulphate aerosol particles is calculated from the mass concentration of aerosol sulphur predicted by the internal sulphur-cycle scheme (see Section 4) using the same assumptions as Jones *et al.* (1994). This reduces to:

$$A_{SO4} = 5.125\times10^{17}\, m \qquad (2)$$

where A_{SO4} is the number of ammonium sulphate aerosol particles (m^{-3}) and m is the total mass concentration of aerosol sulphur (kg m^{-3}).

2.2 Sea-salt

Observations have shown that sea-salt is an important source of CCN in the marine environment (*e.g.* O'Dowd & Smith 1993, Murphy *et al.* 1998). Consequently a simple diagnostic treatment of sea-salt aerosol number concentration was included in the model. Over the sea the number concentration of sea-salt particles was calculated as a function of 10m windspeed (u) using parametrizations based on observational data (O'Dowd *et al.* 1997, 1999a):

For 0 $ms^{-1} \leq u < 2$ ms^{-1}:
$$A_f = 3.856\times10^6 \{1 - \exp(-0.736u)\}$$
$$A_j = 0.671\times10^6 \{1 - \exp(-1.351u)\}$$

For 2 $ms^{-1} \leq u \leq 17.5$ ms^{-1}:
$$\log_{10} A_f = 0.095\, u + 6.283 \qquad (3)$$
$$\log_{10} A_j = 0.0422\, u + 5.7122$$

For $u > 17.5$ ms^{-1}:
$$A_f = 1.5\times10^8 \{1 - 97.874 \exp(-0.313\, u)\}$$
$$A_j = 3.6\times10^6 \{1 - 103.926 \exp(-0.353\, u)\}$$

where A_f and A_j are the number concentrations (m^{-3}) of sea-salt aerosol particles

originating from film and jet droplets respectively, the number concentration being dominated by the sub-micron film particles (see O'Dowd *et al.* 1999a for details). Following evidence from recent field experiments (Noone *et al.* 1996, 1999; O'Dowd *et al.* 1999b) the concentration of these aerosols is assumed to be uniformly mixed throughout the lowest 5 model levels (see Appendix A), although it is admitted that on occasion this may be rather too deep. Above this and over land these quantities are set to zero. As we are currently unable to take account of the size-related properties of sea-salt aerosols (aside from the different formation mechanisms implicit in Eqs. 3), only the total number of sea-salt aerosol particles is used in determining N_d.

The cloud droplet number concentration is determined using the relation of Jones *et al.* (1994) assuming an external mixture of sulphate and sea-salt:

$$N_d = \max\{3.75\times10^8 \, (1 - \exp[-2.5\times10^{-9} \, A]), \, N_{min}\} \qquad (4)$$

where $A = A_{SO4} + A_f + A_j$ and $N_{min} = 5\times10^6$ m^{-3} (but see Section 2.3 below).

2.3 Natural continental CCN

Satellite retrievals of cloud droplet effective radii show a consistent tendency for r_e to be smaller over land than over the ocean (Han *et al.* 1994). In certain areas this difference is due to anthropogenic aerosol sources, but the ubiquity of the land-sea difference suggests that this is not always the only cause. That it might be caused by systematically lower cloud water contents over land is discussed and rejected by Jones & Slingo (1996). Therefore this difference in r_e is plausibly assumed to be at least partially due to naturally-occurring continental sources of CCN (*e.g.* organic aerosols, dust). In the model a crude attempt is made to take some account of this by increasing the minimum droplet concentration N_{min} over ice-free land from 5.0×10^6 to 3.5×10^7 m^{-3}. This value was chosen simply to avoid having lower N_d values over land areas with little or no anthropogenic sulphate emissions when compared with adjacent ocean areas, as such a situation is not generally observed (*e.g.* Pruppacher and Klett 1997, p. 287).

3 Modelling the Indirect Effects of Aerosols

3.1 The first indirect effect

The first indirect effect is modelled by using equations (1)-(4), *i.e.* by allowing the cloud droplet effective radius used in the radiation scheme to be calculated using a variable N_d dependent on aerosol concentration.

3.2 The second indirect effect

As discussed in the introduction, the key process for the second indirect effect is the autoconversion of cloudwater to rainwater. The autoconversion parametrization of the new precipitation scheme (Wilson & Ballard 1999) is based on that of Tripoli & Cotton (1980), and can be thought of as consisting of a 'rate' part and a 'threshold' part. The rate of increase of the mass mixing ratio of rainwater by autoconversion from cloudwater, R_{auto}, is given by:

$$R_{auto} = \frac{0.104\, g\, E_c\, \rho_o^{4/3}}{\mu\, \rho_w^{1/3}} \frac{q_c^{7/3}}{N_d^{1/3}} \qquad (5)$$

where g is the acceleration due to gravity, E_c the collision/collection efficiency of cloud droplets (assumed to be 0.55, Tripoli and Cotton 1980), ρ_o the density of air, q_c the mass mixing ratio of cloud water and μ the dynamic viscosity of air. In the standard version of the scheme the value of N_d is set to 6.0×10^8 m^{-3} over land and 1.5×10^8 m^{-3} over the sea (Bower and Choularton 1992). In order to incorporate the second indirect effect, these fixed values of N_d are replaced by those from Eq. (4).

Autoconversion is allowed to proceed once q_c exceeds a threshold value q_{min}. The value of q_{min} is usually employed as a 'tunable' parameter, and in the standard version of the scheme is set to 3.34×10^{-4} kg kg^{-1} over land and 8.35×10^{-5} kg kg^{-1} over ocean (Wilson and Ballard 1999 and D. R. Wilson, pers. comm.). However, tests indicated a sensitivity of the second indirect effect to the value of this threshold, consistent with the findings of Fowler & Randall (1996) and Rotstayn (1999). Therefore in the version of the model used for this study a different approach was used for determining the autoconversion threshold. Rogers & Yau (1989) suggest that autoconversion will only proceed once the number concentration of cloud droplets greater than 20μm in radius exceeds approximately 1×10^3 m^{-3}. Therefore, following Pruppacher & Klett (1997), a modified gamma cloud droplet size distribution is assumed, and using q_c and N_d as inputs the number concentration of large cloud droplets is calculated. If this is greater than 1×10^3 m^{-3} then autoconversion is allowed to proceed. Consequently N_d, and therefore aerosol

concentration, has a double impact on autoconversion: high values not only suppress R_{auto} *via* Eq. (5), they also increase the autoconversion threshold.

4 The Sulphur Cycle Model

Extra prognostic variables are required to simulate the distribution of sulphate aerosol. The present scheme involves five variables representing the mass mixing ratios of sulphur dioxide (SO_2), dimethyl sulphide (DMS) and three modes of sulphate. The latter comprise two size modes of free particle, labelled Aitken and accumulation modes, and a third mode representing sulphate dissolved in cloud droplets. The free particle modes are assumed to have lognormal size distributions with parameters based on data reported by Quinn *et al.* (1995): the Aitken mode has median radius 24 nm and geometric standard deviation 1.45; the corresponding parameters of the accumulation mode are 95 nm and 1.4. The three modes of sulphate reflect divisions observed in the real atmosphere (*e.g.* by Hoppel *et al.* 1990), and are represented explicitly in order to model their chemical and physical interactions more realistically. For example, the Aitken mode is produced by gas-phase oxidation of SO_2, while the accumulation mode is largely the result of cloud processing (*via* the dissolved mode). Treating the two free modes separately allows size-dependent processes to be represented better, for example in allowing differential rates of dry deposition. Large-scale vertical and horizontal advection of each variable is handled by the model's tracer advection scheme, which uses the flux redistribution method of Roe (1985) to maintain positive definiteness. Vertical transport by convection and turbulent mixing in the boundary layer are also parametrized in ways similar to the model's treatment of the vertical transport of heat and moisture, except that the sulphur variables have no effect on the vertical stability.

The conversion of DMS to SO_2, and of SO_2 to sulphate, requires the parametrization of complex chemistry that is not yet completely understood. The approach taken here is very simple. Monthly average three-dimensional fields of the hydroxyl radical (OH), hydrogen peroxide (H_2O_2) and the peroxide radical (HO_2), produced from simulations using the Lagrangian chemistry model STOCHEM (Collins *et al.* 1997, Stevenson *et al.* 1997), are interpolated in space and time to provide boundary conditions that are used to control the rates of oxidation of DMS and SO_2. The oxidation of DMS is treated in one step, assumed to require the presence of OH, and assumed to yield SO_2 and methyl sulphonic acid (MSA) in constant proportions, presently 90% SO_2 to 10% MSA. (An idea of the high degree of simplification in this can be gained from the 5 of Ravishankara *et al.* 1997. Other models have used various treatments: Lelieveld *et al.* (1997) assumed SO_2 to be the sole product of DMS oxidation; Benkovitz *et al.* (1994) used a temperature-dependent yield ratio; Chin *et al.* (1996) used a more complex mechanism including a hypothetical additional oxidant.) The MSA produced plays no further role in the model and is therefore effectively a sink of sulphur. The rate of oxidation

of DMS (in terms of the decrease in the mass mixing ratio of sulphur as DMS, per second) is given by:

$$d[S_{DMS}]/dt = -9.1\times10^{-12}\,[S_{DMS}][OH] \qquad (6)$$

where $[S_{DMS}]$ is the mass mixing ratio of sulphur as DMS and [OH] is the concentration of OH in units of molecules cm^{-3}.

The conversion of SO_2 to sulphate proceeds *via* two routes: oxidation by OH in the gas phase and by H_2O_2 in solution in cloud droplets. The rate of the gas phase reaction used in the STOCHEM model was adopted here:

$$d[S_{SO2}]/dt = -\,k_{lo}(1 + k_r)^{-1} \times 0.6^{\alpha}\,[S_{SO2}][OH] \qquad (7)$$

where

$$\alpha = \{1 + (0.9693\,\log_{10} k_r)^2\}^{-1}$$

and

$$k_r = k_{lo} / k_{hi}\,.$$

$[S_{SO2}]$ is the mass mixing ratio of sulphur as SO_2. The reaction rate limits at low and high pressure, k_{lo} and k_{hi} respectively, are given by:

$$k_{lo} = 3\times10^{-31}\,N_{air}\,(300 / T)^{3.3}$$

and

$$k_{hi} = 1.5\times10^{-12}$$

where N_{air} is the number of molecules of air per cm^3 and T is the temperature in K. Concentrations of OH are virtually zero at night, so this reaction is then turned off. Accordingly, the daytime average concentration of OH rather than its diurnal average is used in the rate equation.

The aqueous phase reaction is known to proceed on a timescale shorter than the model's timestep of 30 minutes (see, for example, Penkett *et al.* 1979, Hegg & Hobbs 1981 and Snider & Vali 1994). It is also a significant sink of H_2O_2. It is therefore parametrized by converting an amount of SO_2 equal (in molar terms) to the lesser of the concentrations of H_2O_2 and SO_2, and depleting an equal molar amount of H_2O_2. This is done only in the cloudy portion of a grid box, and only in the presence of liquid water (it is assumed that no aqueous phase oxidation takes place in ice cloud). If the concentration of H_2O_2 were reset to its prescribed value on the next timestep there would be a serious overestimate of the rate of aqueous phase oxidation, so instead the H_2O_2 is gradually replenished using the prescribed concentration of HO_2, using the reaction rate used in the

STOCHEM model:

$$d[H_2O_2]/dt = \{2.3\times10^{-13} \exp(600/T) + 1.9\times10^{-33}\, N_{air} \exp(890/T)\} \times \{1 + 1.4\times10^{-21}\, N_{water} \exp(2200/T)\}\, [HO_2]^2 \,. \quad (8)$$

$[H_2O_2]$ is the mass mixing ratio of hydrogen peroxide, N_{water} the number of water molecules per cm^3 and $[HO_2]$ the number of HO_2 molecules per cm^3. As with OH, HO_2 concentrations are negligible after dark, so this replenishment reaction is also turned off at night. In these experiments, in common with others (*e.g.* Chin *et al.* 1996, Kasibhatla *et al.* 1997), aqueous phase oxidation by ozone is omitted. The reaction rate of SO_2 with O_3 is highly *p*H dependent, reducing as more sulphate is produced, so that this reaction has a tendency to be self-limiting. Lohmann & Feichter (1997) found in their modelling studies that between 3% and 12% of the SO_2 was converted by this mechanism annually, although the proportion increased in boreal winter and decreased in summer.

Sulphate produced by aqueous phase oxidation is added to the dissolved sulphate variable, whereas sulphate produced by gas phase oxidation is split between the Aitken and accumulation modes in proportion to their surface areas. The following transfers between the three modes of sulphate are parametrized: (i) evaporation of dissolved sulphate to form accumulation mode sulphate in cloud-free areas; (ii) nucleation of cloud droplets on accumulation mode sulphate in cloud to form dissolved sulphate; and (iii) diffusion of interstitial Aitken mode particles into cloud droplets to form dissolved sulphate. The first two of these processes are assumed to occur on a timescale much shorter than the model timestep, so that any dissolved sulphate in the cloud-free part of the grid box is instantaneously converted to the accumulation mode, and all of the accumulation mode entering cloud is instantaneously converted to dissolved sulphate. The diffusion of Aitken mode sulphate into cloud droplets is a much slower process, and is parametrized using the arguments of Twomey (1977) to obtain an equation for the diffusive lifetime of Aitken mode particles, τ_{diff} :

$$\tau_{diff} = \rho_w^{1/3} (7.8L^{1/3} N_*^{2/3} D)^{-1} \quad (9)$$

where D is a representative diffusion coefficient for Aitken mode particles, taken as 1.71×10^{-9} m^2s^{-1}, and N_* is the number of cloud droplets per unit volume in the standard HadAM3 scheme, *i.e.* 6.0×10^8 m^{-3} over land and 1.5×10^8 m^{-3} over ocean. (There is manifestly some inconsistency here in that N_* is used instead of N_d as predicted by Eq. 4.)

Coagulation of the free particle modes is not represented in the model at present as it occurs on a longer timescale than the other exchange processes, though it is recognised that the omission of coagulation will tend to increase the ratio of Aitken mode sulphate mass to accumulation mode mass in the model. As the deposition efficiencies of

the two modes of particle differ this implies a change in the overall sulphate burden. It is difficult to quantify the exact size of this since the coagulation process is inherently non-linear, but the neglect of coagulation is not considered to be too serious a drawback.

Dry deposition of all of the sulphur species except DMS (for which deposition is neglected) is parametrized using an approach analogous to electrical resistances, similar to many previous studies; see, for instance, the textbook by Seinfeld & Pandis (1998). In the present model, the reference height is effectively at the middle of the layer closest to the surface, and the aerodynamic resistance (r_a) is computed by the stability-dependent boundary-layer mixing scheme. The quasi-laminar resistance (r_b) is computed by first diagnosing the value of r_b for water vapour implied by the boundary-layer/surface scheme, and then scaling this using the relation $r_b \propto D^{-2/3}$, as suggested by Monteith & Unsworth (1990); D is the molecular diffusivity in the case of water vapour and SO_2, or an appropriate particle diffusivity for the free particle modes. The resistance to uptake at the surface (r_c) is set to zero for particles, *i.e.* bouncing-off and resuspension are neglected. For SO_2, r_c is set to zero over ocean; over land it is computed from the stomatal resistance used for water vapour, using the scaling relation $r_c \propto D^{-1}$. The turbulent deposition of sulphate dissolved in cloud droplets (sometimes known as 'occult' deposition) is assumed to be relatively efficient due to the processes of sedimentation and impaction, as discussed by Monteith & Unsworth (1990), so both r_b and r_c are set to zero for this mode.

Because the HadAM3 model treats large-scale cloud and convective cloud separately and quite differently, the parametrization of wet deposition also differs in the two cases. Consider first the treatment of deposition by large-scale precipitation. For precipitation scavenging of SO_2, the rate of removal is assumed to be :

$$d[S_{SO2}]/dt = - 0.18\Psi (1 + 324\ \Psi)^{-1} [S_{SO2}] \qquad (10)$$

where Ψ is the grid-box mean precipitation rate in units of kg m^{-2} s^{-1}. Thus the scavenging coefficient rises linearly with Ψ when the precipitation rate is low, but grows more slowly at high precipitation rates. Rainout of sulphate dissolved in cloud droplets is modelled by assuming that the concentration of dissolved sulphate is uniform within the clouds in a grid box, so that if a certain proportion of the condensed water is removed as precipitation, the same proportion of dissolved sulphate is also removed. If the precipitation completely evaporates before reaching the surface, this removal is suppressed. However the effect of partial evaporation of precipitation below cloud base is not treated; this will clearly tend to overestimate wet deposition. Conversely, scavenging of sulphate particles by falling precipitation ('washout') is not represented, partly to compensate for the aforementioned overestimation and also because it is generally believed to be less important than rainout. (This approximation has been made in some previous studies, for example those of Langner & Rodhe 1991 and Kasibhatla *et al.*

1997). Turning next to scavenging by convective cloud, there is no explicit link with the dissolved sulphate variable as this is associated only with the stratiform cloud. 'Rainout' is therefore not parametrized in the same way: instead both SO_2 and all three modes of particulate sulphate are removed using equation (10), with the additional proviso that for this purpose the convective precipitation is assumed to take place over just 5% of the horizontal area of the grid box. Finally, wet deposition of DMS is not represented at all.

Three sources of atmospheric sulphur are represented in the model. Anthropogenic emissions of SO_2 are taken from the 1B inventory compiled under the auspices of GEIA, the Global Emissions Inventory Activity of IGAC, the International Global Atmospheric Chemistry project (information on GEIA can be found at http://blueskies.sprl.umich.edu/geia). This inventory represents the situation in the mid-1980s, since when emissions have been reduced in many developed countries, such as the United States and most Western European states, but may have increased in some developing nations. Thus the results of the experiments to be described below are not, strictly speaking, representative of present-day conditions. The inventory divides the emissions into those taking place at or very near the surface, and those from elevated sources such as power station chimney stacks. This division is reflected in the model by injecting the elevated emissions directly into the third model layer above the surface (see Appendix A), while the near-surface emissions are introduced as specified surface fluxes in the boundary layer mixing scheme. The global total of the anthropogenic emissions is 67 Tg(S) per annum.

Volcanic emissions are taken from the dataset of Andres & Kasgnoc (1998), also available from GEIA. This inventory is split into contributions from more-or-less continually erupting volcanoes on the one hand and sporadic eruptions on the other. It is not obvious how to handle the effects of the sporadic eruptions in a modelling study that attempts to simulate average conditions. The approach adopted here is to neglect the sporadic volcanoes entirely; thus the estimated indirect anthropogenic forcing will be representative of years when no major (sporadic) eruption occurs. Andres & Kasgnoc estimated that 64% of the global volcanic emissions of sulphur occur in the form of SO_2, with the remainder appearing in a variety of compounds as well as particulate sulphur. For simplicity, these remaining emissions are assumed to occur as SO_2 in the present experiments. The volcanic emissions are injected at a constant rate into layers 4 to 9 of the model, with the mass distributed equally between the layers. The global total of the volcanic emissions is 7.5 Tg(S) per annum.

The other natural source of atmospheric sulphur represented in the model is DMS of biological origin, mainly from the ocean where it is (indirectly) produced by certain species of plankton, as discussed by Liss *et al.* (1997). There is considerable uncertainty regarding the size and distribution of the flux of DMS from the ocean to the atmosphere. This study uses the estimates compiled by Kettle *et al.* (1999), based on measurements of DMS concentrations in seawater made by many workers, combined with climatological

surface wind speeds and the Liss & Merlivat (1986) parametrization of air-sea gas exchange. The seasonal variation in DMS emissions is very important, so the model interpolates in time between fields of monthly mean estimated fluxes. The global marine DMS emission is equivalent to 19.2 Tg(S) per annum. In addition there is a relatively small contribution from the continents, where vegetation and soils emit both DMS and H_2S. For simplicity, these biogenic emissions from land are treated as if they were entirely of DMS. The emissions estimates used are from Spiro *et al.* (1992): the global continental DMS emission is equivalent to 0.9 Tg(S) per annum.

5 Experimental Design

Estimates of the radiative effects of aerosols are usually quoted in terms of *radiative forcing*. This term can be defined as the radiative impact at the top of the atmosphere (TOA) of an instantaneous change in some component of the climate system (in this case, sulphate aerosol concentration), without any subsequent effects of this change being allowed to feed back on the system. However, this approach cannot be taken with the second indirect effect. An instantaneous change in droplet concentration will not instantaneously change the precipitation characteristics of a cloud: these changes must be allowed to feed back to allow the effect to develop. Consequently, to determine the radiative impact of sulphate changes due to this mechanism, a different approach must be taken; the same method is used for the first indirect effect to allow a consistent comparison between the two effects. Pairs of climate model integrations are run in parallel, one using 'pre-industrial' (natural only) sulphate emissions, the other using 'modern' (natural plus anthropogenic) emissions, and the difference in the average TOA net radiation balance between the two runs provides an estimate of the aerosol's radiative impact. As changes due to both indirect effects are allowed to feed back on the climate system, this radiative impact is not, technically speaking, a *forcing*, although the term will occasionally be used in a loose sense. Note that the direct effect of the modelled sulphate aerosol is omitted from all runs. The simulations are run for five years (after an initial 3-month spin-up period) to allow the random changes between the simulations to average out and so let the aerosol-induced signal be seen more clearly.

Nine experiments were conducted, each consisting of two parallel five year runs of the GCM, as follows:

I First indirect effect only;
II Second indirect effect only;
III Second indirect effect only, standard autoconversion threshold;
IV Second indirect effect only, alternative autoconversion rate parametrization;
V Both indirect effects;

VI Both indirect effects, sea-salt parametrization removed;
VII Both indirect effects, standard value of N_{min} used globally;
VIII Both indirect effects, annual-mean aerosol fields;
IX Both indirect effects, seasonal-mean aerosol fields.

Experiments I and II were conducted to determine the magnitude of the first and second indirect effects considered independently. In experiment I the values of droplet number concentration in the precipitation scheme were fixed at the standard values (6.0×10^8 m^{-3} over land and 1.5×10^8 m^{-3} over ocean), and in experiment II (and others investigating only the second indirect effect) the value of cloud droplet effective radius was held fixed at the standard value (7μm) in the radiation scheme. Experiment III, which used the standard method of prescribing the autoconversion threshold, was carried out to assess the impact of the new threshold method described above (see Section 3.2), which was used in all other experiments. The idea of experiment IV was to investigate the degree of uncertainty in the estimation of the second indirect effect caused by the choice of autoconversion rate parametrization. Experiment V was conducted to estimate the total impact of both indirect effects of anthropogenic sulphate: this is effectively the 'main experiment' of the set. The effect of sea-salt aerosols on this estimate was investigated by removing this parametrization in experiment VI. Similarly, the impact of the simple representation of non-sulphate aerosols over land (Section 2.3) was assessed in experiment VII, where the minimum value of cloud droplet number concentration was set to 5.0×10^6 m^{-3} globally. Finally, to assess the importance of using interactive aerosol compared with using prescribed aerosol distributions (as used by Jones & Slingo 1996 and Rotstayn 1999), the sulphate distributions from the pair of runs in experiment V were averaged to create distributions of pre-industrial and modern sulphate. These were then used as boundary conditions for the runs in experiments VIII and IX, the former using 5-year mean sulphate and the latter a seasonal-mean timeseries.

6 Results

The modern and pre-industrial distributions of annual mean total column sulphate from experiment V are shown in Fig. 1. The spatial pattern of the modern distribution is fairly similar to that simulated in previous modelling studies (for instance Langner & Rodhe 1991), with maxima near and downwind of the major industrial source regions. There is a pronounced seasonal cycle, with much higher concentrations of sulphate in summer than in winter. This is mainly due to higher oxidant concentrations in summer (the result of larger fluxes of photolytically-active shortwave radiation), reinforced by the effect of seasonal changes in precipitation. In the map of the pre-industrial sulphate burden, the most prominent maxima are due to volcanic emissions. Because these are injected well above the surface they are subject to less deposition than anthropogenic sulphur and therefore make a relatively larger contribution to the sulphate loading than

might be expected from the total volcanic emission figure, a point well made by Chin & Jacob (1996).

Annual mean concentrations of the dry sulphate mass (*i.e.* the sum of the Aitken and accumulation modes) in the lowest layer of the model, averaged over the five years of experiment V, are compared with measurements near the surface in Tables 1 and 2. Sulphate dissolved in cloud droplets is excluded from the model values for the purposes of this comparison, under the assumption that this would not be sampled by the instruments used to make the measurements. The value at the closest model grid point, or where appropriate the average of the values at two grid points, has been taken.Table 1 contains selected stations from the EMEP* network in Europe; it should be noted that the observations are of total sulphate, *i.e.* the sea-salt sulphate contribution has *not* been subtracted. On the other hand, in Table 2, which contains selected stations from the University of Miami database (Savoie and Prospero, personal communication, 1999), the values are of non-sea-salt sulphate. The EMEP data have in each case been averaged over the 4 years 1986-89 inclusive. Data for subsequent years are available, but have been excluded from the comparison because of the significant changes in European emissions that have taken place since 1990: recall that the anthropogenic emissions inventory represents the position in the mid-1980s. In most cases inclusion of post-1989 EMEP data would have spuriously improved the agreement between the model and the

TABLE 1. Comparison of annual-mean sulphate concentrations in the lowest layer of the model, taken from experiment V, with measurements at stations in the EMEP network. Units are μg (SO_4) m^{-3}

Station	Location	Period	Measured	Simulated
Stoke Ferry (GB4)	52° 34′ N 0° 30′ E	86-89	5.94	2.12
Toledo (ES1)	39° 33′ N 4° 21′ W	86-89	1.79	2.06
Tustervatn (NO15)	65° 50′ N 13° 55′ E	86-89	1.25	0.42
Rorvik (SE2)	57° 25′ N 11° 56′ E	86-89	4.47	1.00
Langenbrugge (DE2)	52° 48′ N 10° 45′ E	86-89	7.08	3.15
Deuselbach (DE4)	49° 46′ N 7° 03′ E	86-89	5.49	3.77
Hof (DE20)	50° 19′ N 11° 53′ E	86-89	7.17	4.16
Ispra (IT4)	45° 48′ N 8° 38′ E	86-89	8.58	3.65
Jarczew (PL2)	51° 19′ N 21° 59′ E	86-89	12.9	3.61
K-puszta (HU2)	46° 58′ N 19° 35′ E	86-89	4.62	6.20
Aliartos (GR1)	38° 22′ N 23° 05′ E	86-89	5.07	3.22

* Co-operative Programme for Monitoring and Evaluation of the Long Range Transmission of Air Pollutants in Europe

TABLE 2. Comparison of annual-mean sulphate concentrations in the lowest layer of the model, taken from Experiment V, with measurements from the Miami University dataset. Units are μg (SO_4) m^{-3}

Station	Location	Period	Measured	Simulated
Mace Head	53.32° N 9.85° W	88-94	1.28	0.607
Barbados	13.17° N 59.43° W	84-98	0.758	0.291
Midway	28.22° N 177.35°W	81-97	0.52	0.270
Oahu	21.33° N 157.70°W	81-95	0.51	0.279
Fanning	3.92° N 159.33° W	81-86	0.64	0.111
American Samoa	14.25° S 170.58° W	83-96	0.343	0.285
New Caledonia	22.15° S 167.00° E	83-85	0.436	0.190
Norfolk Island	29.08° S 167.98° E	83-97	0.273	0.168
Cape Grim	40.68° S 144.68° E	83-96	0.297	0.163
Wellington/Baring Hd	41.28°S 174.87° E	87-96	0.43	0.152
Chatham Island	43.92° S 176.50° W	83-96	0.27	0.126
East Falkland	51.75° S 60.00° W	87-96	0.393	0.0827
Mawson, Antarctica	67.60° S 62.50° E	87-96	0.112	0.0126

observations; for example, at Deuselbach in Germany the average over the following 4 year period, 1990-1993, was 3.8 μg (SO_4) m^{-3}. (A major exception to this is at Aliartos in Greece, where concentrations rose sharply to 20.3 μg (SO_4) m^{-3} averaged over 1990-1993). The data in Table 2 have been averaged over various periods, as shown. Stations in the University of Miami database that may be affected by local sources, or that were not operational during at least some part of the 1980s, have been excluded. Both tables indicate that the model predicts lower sulphate concentrations than are observed. As a rough generalisation the discrepancy between model and observations tends to be wider in regions remote from anthropogenic sources, an extreme example being Mawson in Antarctica, though one can find exceptions to this trend.

The global annual mean aerosol burdens in experiment V are equivalent to approximately 0.094 Tg(S) in the pre-industrial case and 0.36 Tg(S) in the modern case. These are smaller than in most previous modelling studies, for example the model of Lelieveld *et al.* (1997) produced 1.05 Tg(S), the model of Roelofs *et al.* (1998) produced 0.96 Tg(S), the model of Pham *et al.* (1995) produced 0.80 Tg(S), the model of Feichter *et al.* (1996) produced 0.63 Tg(S), the model of Chuang *et al.* (1997a) produced 0.55 Tg(S) and the model of Chin & Jacob (1996) produced 0.53 Tg(S), in each case using both natural and anthropogenic emissions. While there is some variation in the emissions datasets used in these studies, much of the range in aerosol loading is likely to be due to

differences in the formulation of the models. Lelieveld *et al.*(1997) comment that underestimation of sulphate concentrations is a common problem in 3D models, and suggest that other oxidation mechanisms, such as heterogeneous reactions on mineral dust, may be important.

The relatively low sulphate burdens in the present study appear to be associated with the following features of the model:

(i) non-inclusion of aqueous phase oxidation by ozone and in supercooled water droplets;
(ii) lack of release of aerosol from partial evaporation of precipitation in the wet scavenging parametrization;
(iii) use of a fixed cloud droplet number concentration in the in-cloud scavenging parameterization of the Aitken mode;
(iv) excessive dry deposition of SO_2 when the boundary layer is stable;
(v) non-inclusion of sulphate 'emissions' due to instantaneous oxidation of SO_2 at source (as in Lelieveld *et al.* 1997);
(vi) the rainout parametrization using an explicit dissolved sulphate variable;
(vii) the gradual replenishment of H_2O_2 after its depletion during aqueous phase oxidation.

The first four of these are evidently areas where further model developments are called for; the fifth could easily be included, but it is not clear that it can be justified. The final two features may, in principle, be good: the importance of the last of these was well brought out by Roelofs *et al.* (1998). One additional factor that affects only the natural sulphate concentration is that the DMS oxidation scheme excludes a pathway that yields SO_3 (and hence very rapidly H_2SO_4) without passing through SO_2 as an intermediate (see Figure 7 of Ravishankara *et al.* 1997).

The model's simulation of cloud droplet effective radius was assessed by comparing it with the retrievals of Han *et al.* (1994). The modelled distribution of r_e was taken from the run using modern sulphur emissions in experiment V. A composite distribution of the retrieved r_e was produced by taking the mean of the retrievals from January, April, July and October 1987. This was compared with a similar composite from the model, using the 5-year mean r_e values from the same 4 months. As the same missing-data mask was applied to both distributions this limits the comparison to approximately 50°N to 40°S, the latitudinal range of the composite satellite retrievals. The comparison is shown in Fig. 2 and tabulated in Table 3 (all values in microns).

TABLE 3. Comparison between modelled and retrieved values of cloud droplet effective radius (μm) from experiment V.

	Model	Retrieval
Global (50°N to 40°S only)	12.3	10.6
Northern hemisphere	11.6	9.9
Southern hemisphere	13.0	11.4
Ocean	13.2	11.7
Land	10.1	7.6

Although generally within the 1-2μm uncertainty of the Han *et al.* retrievals, there is clearly a tendency for the model to overpredict the value of r_e, most noticeably over land, suggesting that droplet concentrations in the model are too low. This is consistent with the generally low sulphur burden in the model and with the fact that only sulphate and sea-salt aerosols are modelled in any detail.

The impact of anthropogenic sulphate aerosols on top-of-atmosphere reflected shortwave, outgoing longwave and total net radiation (positive defined as downwards for the net radiation) in the nine experiments, averaged over the five years of the runs, is given in Table 4 (values are presented as modern minus pre-industrial and are in units of Wm^{-2}). The ranges quoted are the standard deviations obtained by treating the individual annual-means of the 5-year simulations as independent samples.

TABLE 4. Changes in reflected shortwave (RSW), outgoing longwave (OLR) and top-of-atmosphere net downward radiation (Net TOA) on going from pre-industrial to modern sulphur emissions (Wm^{-2})

	Experiment	Δ RSW	Δ OLR	Δ Net TOA
I	1st indirect effect only	+0.98	−0.14	−0.84 ± 0.09
II	2nd indirect effect only	+0.76	−0.14	−0.62 ± 0.23
III	2nd ind. eff., old autoconv. threshold	+0.62	−0.08	−0.55 ± 0.13
IV	2nd ind. eff., Beheng autoconv. rate	+2.59	−0.55	−2.05 ± 0.19
V	Both indirect effects	+1.25	−0.20	−1.05 ± 0.18
VI	Both indirect effects, no sea-salt	+1.62	−0.29	−1.33 ± 0.26
VII	Both effects, N_{min} = 5 cm^{-3} globally	+1.79	−0.36	−1.42 ± 0.12
VIII	Both effects, annual-mean sulphate	+2.07	−0.43	−1.64 ± 0.04
IX	Both effects, seasonal-mean sulphate	+2.03	−0.35	−1.68 ± 0.20

The distributions of the indirect radiative impacts from experiments I, II and V are shown in Fig. 3. There are forcing maxima adjacent to the main sources of sulphur emissions in the North-Eastern USA, Europe and China, and also off the west coasts of both North and South America. In many cases the forcing tends to be concentrated over the oceans reflecting the distribution of low-level liquid-water cloud in the model. The global mean for the total indirect effect (Fig. 3c) of -1.05 Wm^{-2} is similar to the value obtained by Hansen *et al.* (1998) who estimated the effect of aerosols on clouds by considering the observed change in the diurnal range of surface temperature.

Comparing the sum of the impacts of each effect separately (experiments I and II) with that of both effects simultaneously (experiment V) it is clear that the effects do not add linearly - the sum of I and II overestimates the total impact (V) by some 40%. As both effects tend to have an impact in the same areas, as shown in Fig. 3, there will tend to be a degree of saturation of the effects contributing to this lack of a cumulative impact.

Comparing the results of experiments II and III shown in Table 4 indicates that using the standard threshold in the autoconversion tends to lead to a somewhat lower (by ~10%) estimate of the second indirect effect. Although this difference is not great, it is probably preferable to use the new threshold parametrization which has a somewhat more physical basis.

An indication of the uncertainty associated with estimates of the second indirect effect can be seen by comparing the results of experiments II and IV. These had the same method of calculating the autoconversion threshold, but in IV the autoconversion rate parametrization used by Lohmann & Feichter (1997) in the ECHAM model (Beheng 1994) was used instead of the standard parametrization (Eq. 5). As used by Lohmann & Feichter, this alternative rate parametrization gives R_{auto} as:

$$R_{auto} = \gamma_1 \, 6\times10^{28} \, n^{-1.7} \, (N_d \times 10^{-6})^{-3.3} \, (\rho_o \, q_c \times 10^{-3})^{4.7} \, \rho_o^{-1} \qquad (11)$$

where γ_1 is a tunable efficiency parameter (=220) and n is a parameter related to the droplet spectrum width (=10); the other quantities are as before. Clearly the Beheng scheme has a stronger dependence on cloud water content and droplet concentration compared with the standard scheme, and so not surprisingly the use of this parametrization leads to an increase in the second indirect effect by a factor of about 3.3.

Experiments VI and VII both show an increase in the total indirect radiative impact when compared with experiment V. This is because both experiments act to remove a component of the natural (or 'background') aerosol distribution, thereby increasing the susceptibility of clouds to anthropogenic influence. Comparing experiments VI and V shows that neglecting sea-salt aerosol increases the impact of the indirect effects by about 27%. This is a somewhat larger effect than has been seen previously with fixed

sulphate distributions, where the impact was of order 10% (Jones & Slingo 1997), but the impact of sea-salt also depends very much on the background sulphate distribution. To examine the sensitivity of the impact of sea-salt to the number of layers through which the sea-salt is distributed, an additional experiment was performed in which the sea-salt was only distributed through the lowest 3 layers (up to ~900mb) as opposed to the standard 5 layers (up to ~750mb). This increased the total radiative impact of anthropogenic sulphate by about 15% compared with the value obtained in experiment V, indicating some sensitivity to the assumed depth of the atmosphere influenced by sea-salt. However, the standard assumption of mixing through the full depth of the model's boundary layer (*i.e.* to ~750 mb) was deemed acceptable as the sea-salt number concentration is dominated by film-mode particles of mean radius 0.1 μm which could easily be mixed to that height. Further, the important conditions from a radiative point of view are those of high wind speed: the conditions which generate significant numbers of sea-salt particles are precisely those which will tend to favour the generation of deep, well-mixed boundary layers. The effect of removing the simple representation of non-sulphate aerosols over land (VII *vs.* V) has somewhat more of an impact, increasing the change in TOA net radiation by about 35% because of the large anthropogenic increases in sulphate loading over land. Both these experiments emphasise the importance of the natural background cloud droplet distribution in attempting to estimate the indirect effects.

Comparing the radiative impacts from experiments V with those from experiments VIII and IX indicates the considerable impact of using prescribed sulphate distributions. By design these three experiments have the same annual-mean sulphate burdens, yet the radiative impact determined using non-interactive prescribed aerosol fields (VIII and IX) overestimates the total indirect effect by approximately 60%, even when seasonally-varying distributions are used (IX). This would seem to indicate a strong preference for the interactive modelling of aerosols within GCMs. This result is somewhat stronger than that noted previously by Feichter *et al.* (1997). They found an increase of 20% in the indirect forcing when using time-mean sulphate fields, but the results are not strictly comparable: Feichter *et al.* considered only the first indirect effect and used monthly-mean sulphate data, whereas here we consider both indirect effects and use seasonal- or annual-mean sulphate.

The changes in shortwave (SWCF) and longwave (LWCF) cloud forcings from the nine experiments, averaged over the 5 years of the runs, are given in table 5 (in units of Wm^{-2}); note that when considering cloud forcing the sign convention is that downwards is positive for both shortwave and longwave radiation. Also given are the associated percentage changes in global annual-mean cloud liquid water path (LWP) and the absolute change in percentage cloud cover.

TABLE 5. Pre-industrial to modern-day changes in shortwave and longwave cloud forcing (Wm^{-2}), the percentage change in global annual mean cloud liquid water path and the absolute change in percentage cloud cover

	Experiment	Δ SWCF	Δ LWCF	Δ LWP	Δ Cloud
I	1st indirect effect only	−0.91	0.00	−0.13	+0.11
II	2nd indirect effect only	−0.78	+0.12	+4.53	+0.47
III	2nd ind. eff., old autoconv. threshold	−0.61	+0.08	+2.47	+0.23
IV	2nd ind. eff., Beheng autoconv. rate	−2.55	+0.26	+20.62	+1.44
V	Both indirect effects	−1.28	+0.10	+3.40	+0.35
VI	Both indirect effects, no sea-salt	−1.59	+0.14	+6.74	+0.56
VII	Both effects, N_{min} = 5 cm^{-3} globally	−1.69	+0.16	+5.46	+0.66
VIII	Both effects, annual-mean sulphate	−2.02	+0.22	+6.04	+0.80
IX	Both effects, seasonal-mean sulphate	−1.98	+0.13	+6.70	+0.66

Apart from the very small changes in experiment I, there is a roughly linear relationship between the changes in LWP and in cloud cover. There is no systematic change in column-integrated water vapour (not shown): of the 9 experiments there are 4 increases (mean +0.15%) and 5 decreases (mean −0.21%) in modern-day column-integrated water vapour compared with their respective pre-industrial simulations. Apart from experiment II, which had a slight increase in global-mean surface temperature (+0.007K), the modern-day simulations of all other experiments had global-mean surface temperatures which were cooler than their respective pre-industrial simulations (mean cooling −0.055 ± 0.025 K). However, given that these simulations are only for 5 years and do not have an interactive ocean (*i.e.* they have climatological sea-surface temperatures), these results are at best qualitative.

Whether one considers the changes in TOA net radiation (Table 4) or in net cloud forcing (Table 5), these results indicate that, for the second indirect effect, the shortwave 'cooling' effect due to brighter clouds far outweighs the longwave 'warming' effect due to higher LWPs. This is because the longwave cloud forcing associated with the types of low-level liquid water clouds under consideration here is weak compared with their short-wave forcing.

The change of −1.28 Wm^{-2} in shortwave cloud forcing caused by both effects together (experiment V) is comparable with the value of −1.4 Wm^{-2} obtained by Lohmann & Feichter (1997), who also used an interactive sulphur cycle. However, these similar values are obtained using different autoconversion rate schemes. When the model is modified to use the same parametrization as ECHAM4 (Eq. 11) the change in net cloud

forcing due solely to the second indirect effect strengthens from −0.66 to −2.29 Wm^{-2} (experiments II and IV). The very large change in LWP associated with the Beheng parametrization is evident in the values shown in Table 5: whilst all other experiments which include the second indirect effect show an increase in LWP of the order of 5%, experiment IV shows an increase of slightly over 20%. This is broadly consistent with the 17.1% LWP increase obtained by Lohmann & Feichter.

A somewhat larger total indirect radiative effect of −2.1 Wm^{-2} was obtained by Rotstayn (1999) using a version of the CSIRO model. Rotstayn obtained an increase in LWP of a similar order of magnitude (6%) to those shown in Table 5 (with the exceptions of experiments I and IV), which is consistent with the use in the CSIRO model of the same autoconversion rate parametrization as used here.

7 Discussion and Conclusions

A series of experiments has been conducted to make estimates of the total indirect effect of anthropogenic sulphate aerosols, both *via* increases in cloud albedo and *via* changes to the precipitation efficiency of clouds. The experiments used a version of the HadAM3 GCM with an interactive sulphur cycle, a diagnostic treatment of sea-salt aerosol and a new cloud microphysics scheme. The conclusions from the experiments are:

1. that the second indirect effect is of similar magnitude to the first;
2. that the two effects do not add linearly;
3. that the shortwave (cooling) impact of the second effect dominates its longwave (warming) impact;
4. that estimating indirect forcing using non-interactive aerosol fields can introduce a significant error;
5. that the total indirect radiative impact of anthropogenic sulphate aerosols is approximately −1 Wm^{-2};
6. that this value is uncertain to within at least a factor of 2.

The uncertainty in the value of the total indirect effect is associated both with the 'inputs' (*i.e.* the specification of the aerosol distribution) and with the 'processes' (*i.e.* the parametrization schemes). The sulphate and sea-salt aerosols which are modelled explicitly in this study (one prognostically and one diagnostically) are only two components of the atmospheric aerosol which is usually much more complex in composition. Other species which are of importance include carbonaceous aerosols (both organic and inorganic), nitrates and mineral dust, many of which occur as components of CCN. The impact of these non-sulphate aerosols depends on the relative

degree to which they affect the pre-industrial and the modern concentration of cloud droplets, *i.e.* to what degree they are natural or anthropogenic. For example, the results presented here suggest that ignoring the contribution of sea-salt to the distribution of CCN can cause an overestimate of the total indirect effect of about 27%. Even considering sulphate alone there is considerable uncertainty, with significant differences between different models. There are strong indications that the present model underestimates the atmospheric sulphate aerosol concentrations, which is bound to have a large impact on the estimated indirect effects. Related to the question of aerosol composition is that of the relationship between aerosol and cloud droplet number concentrations. Improvements to the relations currently used will require a greater understanding of the complex processes involved in cloud nucleation (*e.g.* Chuang *et al.* 1997b, Hallberg *et al.* 1998) as well as improvements in the modelling of the CCN distribution used as input.

Further sources of uncertainty are illustrated by the experiments which use different parametrizations of the autoconversion rate. These demonstrate a significant sensitivity of the second indirect effect to this process, with the capacity to double the estimate of the radiative impact of the effect. It is still early days for the representation of cloud microphysics in GCMs, and there is clearly considerable work to be done in improving our understanding of such complex and highly non-linear processes as autoconversion. The fact that we find similar degrees of uncertainty associated with both 'inputs' and 'processes' differs from the conclusion of Pan *et al.* (1998) who found a far larger uncertainty connected with the inputs ('parametric uncertainty') compared with the processes ('structural uncertainty'). However, their study was concerned only with the first indirect effect, and the large 'structural uncertainties' we find are associated with the parametrization of autoconversion which is central to the second indirect effect.

Conclusion 4 is important in view of the fact that most of the early attempts to estimate the (first) indirect effect used non-interactive aerosol fields; for example, Jones *et al.* (1994) used annual-mean sulphate data. It suggests that if climate or numerical weather prediction models are to include schemes in which cloud properties are allowed to depend on aerosol distributions, the use of prescribed aerosol climatologies may give unsatisfactory results *even if the climatologies themselves are reliable*. The fundamental reason for this is that the relation between the aerosol and cloud droplet concentrations is nonlinear, so that using input aerosol concentrations meaned over any period longer than the timescale on which aerosols evolve will introduce an error. Appendix B discusses this question in more depth, and contains an argument explaining how the exact form of the parameterization linking the aerosol and cloud droplet concentrations (Eq. 4) leads to magnified estimates of the size of the indirect effect in the experiments with prescribed sulphate distributions (VIII and IX). The opposite possibility, that alternative parameterizations might, when driven by non-interactive aerosol fields, yield estimates of the size of the indirect effect that are too small, cannot be excluded. However, since any physically reasonable parameterization will be nonlinear, the use of

non-interactive aerosol fields is highly likely to introduce significant error (barring a fortuitous cancellation of the errors in the pre-industrial and anthropogenically-perturbed cases).

Nevertheless, despite these uncertainties, these results suggest that the indirect effects of aerosols on clouds are important and that they should be taken into account when considering human influence on climate: the estimate of -1.05 Wm^{-2} for the total indirect effect would offset approximately 40% of the forcing caused by the increases in greenhouse gases to date.

8 Current and Future Work

One area where the model described here clearly requires improvement is that of the simulation of sulphate aerosol concentrations: as can be clearly seen in Tables 1 and 2, the model underpredicts the near-surface concentration of sulphate, especially in regions remote from centres of pollution. Preliminary studies using the next version of the Hadley Centre model (HadAM4), which has, amongst other things, higher vertical resolution and an improved boundary-layer scheme, have shown significant improvements in the simulation of sulphate concentrations. Some of the deficiencies in the sulphur cycle noted in Section 4 have also been corrected, and the simulated values in the new model are in far better agreement with the observations, especially in remote regions. The new model also has increased amounts of cloud cover, bringing it into closer agreement with satellite observations, and the combination of these changes has lead to an increase in the total indirect effect of between 25 and 30%.

Future work on the sulphur cycle will involve further improvement of the scheme along the lines indicated in Section 4. Information from observational campaigns such as ACE-2 will be used to try to improve the representation of the various aerosol and cloud microphysical processes underlying the indirect effects, and work will also continue on developing schemes to represent other species of aerosol.

Acknowledgements We are grateful to D. L. Savoie and J. M. Prospero (Rosenstiel School of Marine and Atmospheric Science, University of Miami) for permission to cite data from their aerosol database. We are equally grateful to those involved in assembling the EMEP dataset. We wish to thank our colleague C. E. Johnson for his help in producing the oxidant fields from STOCHEM. This work was supported by the UK Department of the Environment, Transport and the Regions under contract PECD 7/12/37.

Appendix A

Vertical co-ordinates of the Hadley Centre model

The GCM uses a hybrid vertical co-ordinate system which varies smoothly from a pure sigma co-ordinate (pressure divided by surface pressure) near the surface to a pure pressure system towards the top of the model. Pressure (*p*) at a given level is given by:

$$p = A + Bp^*,$$

where p^* is the surface pressure (Pa). The values of the coefficients A and B for the boundaries of the model layers are given below with boundary 0 indicating the surface:

Boundary	A	B
19	50.0	0.0
18	1000.0	0.0
17	2000.0	0.0
16	4000.0	0.0
15	7176.0	0.003239
14	10652.1	0.018478
13	12997.5	0.045024
12	14342.7	0.081572
11	14818.3	0.126816
10	14555.1	0.179448
9	13447.6	0.250523
8	11175.3	0.348246
7	7727.9	0.472720
6	3852.2	0.611477
5	939.0	0.740609
4	0.0	0.835
3	0.0	0.905
2	0.0	0.956
1	0.0	0.994
0	0.0	1.0

Appendix B

The aim of this appendix is to shed some light on the question of why using prescribed time-average aerosol fields produces estimates of indirect effects that are in general different from, and in the particular case of the present study stronger than, those obtained with interactive aerosol fields. The arguments to be presented are not a proof, but they do provide useful insight into the behaviour of the model.

The discussion revolves around the form of the function linking cloud droplet number concentration N_d with the aerosol number concentration A. Reduced to its mathematical essentials, this is:

$$N_d(A) = N_\infty (1 - e^{-\lambda A}) \qquad \text{if } A > A_m,$$
$$N_d(A) = N_m \qquad \text{if } 0 \leq A \leq A_m.$$

Here N_m is the minimum value of N_d at low aerosol concentrations, N_∞ is the asymptotic limit of N_d as $A \rightarrow \infty$, λ is a constant and A_m is such that $N_m = N_\infty (1 - e^{-\lambda A_m})$.

For $A > A_m$,

$$N_d''(A) = -\lambda^2 N_\infty e^{-\lambda A} < 0,$$

so that the function is concave (for $A > A_m$). Now for a concave function $f(x)$, with x taking on a distribution of values either in space, time or as a random variable, and with an asterisk denoting an average or probabilistic expectation, Jensen's inequality states that:

$$f(x^*) \geq \{f(x)\}^*$$

i.e. using the mean value of x as input to f produces an output that overestimates the true mean of f. (Actually, Jensen's inequality is normally proved for *convex* functions, in which case the direction of the inequality is reversed; see *e.g.* Feller 1966.)

Thus in the anthropogenically-perturbed situation where $A >> A_m$ most of the time, it is to be expected that $N_d(A^*) > \{N_d(A)\}^*$, *i.e.* using the mean aerosol concentration will *over*estimate the true average droplet concentration.

In contrast, if $A < A_m$ then $N_d(A)$ is not concave. Indeed, if $A^* \leq A_m$ then $N_d(A^*) = N_m \leq \{N_d(A)\}^*$, *i.e.* using the mean aerosol concentration will *under*estimate the true average droplet concentration. This situation is likely to occur quite frequently in the pre-industrial experiments. The result of a tendency to underestimate N_d in the pre-industrial case and overestimate it in the modern case would be that the size of the

indirect effect would be exaggerated.

If $A^* > A_m$ but the distribution of A does extend significantly below A_m, then it seems that no general statement about the relative sizes of $N_d(A^*)$ and $\{N_d(A)\}^*$ can be made (without making further assumptions about the distribution of A). Therefore it is difficult to *prove* that using average aerosol fields must exaggerate the strength of indirect forcing. However, the above arguments make it very plausible that this is likely to occur when N_d is parametrized in the way chosen here.

Some further comments may be appropriate. First, although there is much uncertainty about the best way to parametrize the relation between A and N_d, one would expect the concavity property to be realistic: as A increases, the competition between the different aerosol particles for the available water vapour will result in N_d rising more and more slowly. Secondly, the use of a minimum cloud droplet number concentration N_m is the key element that causes the error in estimating the indirect effect using average aerosol fields to be an *over*estimate. If $N_d(A)$ were concave everywhere, then the cloud droplet number concentration would be overestimated in both the anthropogenically-perturbed and pre-industrial experiments (with mean aerosol). In that case the error due to using specified time-average fields could take either sign; one would nevertheless anticipate a significant error unless the averaging period were so small as to be comparable with the timescale on which aerosol fields evolve. Any averaging period greater than a day is unlikely to be adequate.

References

Ackerman, A. S., Toon, O. B. and Hobbs, P. V., 1995. Numerical modelling of ship tracks produced by injection of cloud condensation nuclei into marine stratiform clouds. *J. Geophys. Res.*, **100**, 7121-7133

Albrecht, B. A., 1989. Aerosols, cloud microphysics and fractional cloudiness. *Science*, **245**, 1227-1230

Andres, R. J. and Kasgnoc, A. D., 1998. A time-averaged inventory of subaerial volcanic sulfur emissions. *J. Geophys. Res.*, **103**, 25251-25261

Beheng, K. D., 1994. A parameterization of warm cloud microphysical conversion processes. *Atmos. Res.*, **33**, 193-206

Benkovitz, C. M., Berkowitz, C. M., Easter, R. C., Nemesure, S., Wagener, R. and Schwartz, S. E., 1994. Sulfate over the North Atlantic and adjacent continental regions: Evaluation for October and November 1986 using a three-dimensional model driven by observation-derived meteorology. *J. Geophys. Res.*, **99**, 20725-20756

Boucher, O. and Lohmann, U., 1995. The sulfate-CCN-cloud albedo effect: A sensitivity study with two general circulation models. *Tellus B*, **47**, 281-300

Bower, K. N. and Choularton, T. W., 1992. A parametrisation of the effective radius of ice free clouds for use in global climate models. *Atmos. Res.*, **27**, 305-339

Chin, M. and Jacob, D. J., 1996. Anthropogenic and natural contributions to tropospheric sulfate: a global model analysis. *J. Geophys. Res.*, **101**, 18691-18699

Chin, M., Jacob, D. J., Gardner, G. M., Foreman-Fowler, M. S., Spiro, P. A. and Savoie, D. L.,1996. A global three-dimensional model of tropospheric sulfate. *J. Geophys. Res.*, **101**, 18667-18690

Chuang, C. C., Penner, J. E., Taylor, K. E., Grossman, A. S. and Walton, J. J., 1997a. An assessment of the radiative effects of anthropogenic sulfate. *J. Geophys. Res.*, **102**, 3761-3778

Chuang, P. Y., Charlson, R. J. and Seinfeld, J. H., 1997b. Kinetic limitations on droplet formation in clouds. *Nature*, **390**, 594-596

Collins, W. J., Stevenson, D. S., Johnson, C. E. and Derwent, R. G., 1997. Tropospheric ozone in a global-scale three-dimensional Lagrangian model and its response to NO_x emission controls. *J. Atmos. Chem.*, **26**, 223-274

Cox, P. M., Betts, R. A., Bunton, C. B., Essery, R. L. H., Rowntree, P. R. and Smith, J., 1999. The impact of new land surface physics on the GCM simulation of climate and climate sensitivity. *Clim. Dyn.*, **15**, 183-203

Cullen, M. J. P., 1993. The unified forecast/climate model. *Meteorol. Mag.*, **122**, 81-94

Durkee, P. A., Noone, K. J., Ferek, R. J., Johnson, D. W., Taylor, J. P., Garrett, T. J., Hobbs, P. V., Hudson, J. G., Bretherton, C. S., Innis, G., Frick, G. M., Hoppel, W. A., O'Dowd, C. D., Russell, L. M., Gasparovic, R., Nielson, K. E., Öström, E., Osborne, S. R., Flagan, R. C., Seinfeld, J. H. and Rand, H., 1999. The impact of ship-produced aerosols on the microphysical characteristics of warm stratocumulus clouds: A test of MAST hypotheses 1.1a and 1.1b. *J. Atmos. Sci.*, **56** (in press)

Edwards, J. M. and Slingo, A., 1996. Studies with a flexible new radiation code. I: Choosing a configuration for a large-scale model. *Q. J. R. Meteorol. Soc.*, **122**, 689-719

Feichter, J., Lohmann, U. and Schult, I., 1997. The atmospheric sulfur cycle in ECHAM-4 and its impact on the shortwave radiation. *Clim. Dyn.*, **13**, 235-246

Feichter, J., Kjellström, E., Rodhe, H., Dentener, F., Lelieveld, J. and Roelofs, G.-J.,1996. Simulation of the tropospheric sulfur cycle in a global climate model. *Atmos. Environ.*, **30**, 1693-1707

Feller, W., 1966. *An Introduction to Probability Theory and Its Applications, volume II.* John Wiley & Sons, New York

Ferek, R. J., Garrett, T., Hobbs, P. V., Strader, S., Johnson, D. W., Taylor, J. P., Nielson, K., Ackerman, A. S., Kogan, Y., Liu, Q., Albrecht, B. A. and Babb, D., 1999. Drizzle suppression in shiptracks. *J. Atmos. Sci.*, **56** (in press)

Fowler, L. D. and Randall, D. A., 1996. Liquid and ice cloud microphysics in the CSU general circulation model. Part III: Sensitivity to modeling assumptions. *J. Clim.*, **9**, 561-586

Gregory, D., Kershaw, R. and Inness, P. M., 1997. Parametrization of momentum transport by convection. II: Tests in single-column and general circulation models. *Q. J. R. Meteorol. Soc.*, **123**, 1153-1183

Hallberg, A., Noone, K. J. and Ogren, J. A., 1998. Aerosol particles and clouds: which particles form cloud droplets? *Tellus B*, **50**, 59-75

Han, Q., Rossow, W. B. and Lacis, A. A., 1994. Near-global survey of effective droplet radii in liquid water clouds using ISCCP data. *J. Clim.*, **7**, 475-497

Hansen, J. E., Sato, M., Lacis, A., Ruedy, R., Tegen, I. and Matthews, E., 1998. Climate forcings in the industrial era. *Proc. Natl. Acad. Sci. USA*, **95**, 12753-12758

Hegg, D. A. and Hobbs, P. V., 1981. Cloud water chemistry and the production of sulfates in clouds. *Atmos. Environ.*, **15**, 1597-1604

Hegg, D. A., Livingston, J., Hobbs, P. V., Novakov, T. and Russell, P., 1997. Chemical apportionment of aerosol column optical depth off the mid-Atlantic coast of the United States. *J. Geophys. Res.*, **102**, 25293-25303

Heymsfield, A. J., 1977. Precipitation development in stratiform ice clouds: A micro-physical and dynamical study. *J. Atmos. Sci.*, **34**, 367-381

Hoppel, W. A., Fitzgerald, J.W., Frick, G. M., Larson, R. E. and Mack, E. J., 1990. Aerosol size distributions and optical properties found in the marine boundary layer over the Atlantic Ocean. *J. Geophys. Res.*, **95**, 3659-3686

Hudson, J. G. and Li, H., 1995. Microphysical contrasts in Atlantic stratus. *J. Atmos. Sci.*, **52**, 3031-3040

IPCC 1996. *Climate Change 1995: The science of climate change* (eds. J. T. Houghton, L. G. Meira Filho, J. Bruce, H. Lee, B. A. Callander, E. Haites, N. Harris and K. Maskell). Cambridge University Press

Johns, T. C., Carnell, R. E., Crossley, J. F., Gregory, J. M., Mitchell, J. F. B., Senior, C. A., Tett, S. F. B. and Wood, R. A., 1997. The second Hadley Centre coupled ocean-atmosphere GCM: Model description, spinup and validation. *Clim. Dyn.*, **13**, 103-134

Jones, A., Roberts, D. L. and Slingo, A., 1994. A climate model study of indirect radiative forcing by anthropogenic sulphate aerosols. *Nature*, **370**, 450-453

Jones, A. and Slingo, A., 1996. Predicting cloud droplet effective radius and indirect sulphate aerosol forcing using a general circulation model. *Q. J. R. Meteorol. Soc.*, **122**, 1573-1595

Jones, A. and Slingo, A., 1997. Climate model studies of sulphate aerosols and clouds. *Phil. Trans. R. Soc. Lond. B*, **352**, 221-229

Kasibhatla, P., Chameides, W. L. and St. John, J., 1997. A three-dimensional global model investigation of seasonal variations in the atmospheric burden of anthropogenic sulfate aerosols. *J. Geophys. Res.*, **102**, 3737-3759

Kettle, A. J., Andreae, M. O., Amouroux, D., Andreae, T. W., Bates, T. S., Berresheim, H., Bingemer, H., Boniforti, R., Helas, G., Leck, C., Maspero, M., Matrai, P., McTaggart, A. R., Mihalopoulos, N., Nguyen, B. C., Novo, A., Putaud, J. P., Rapsomanikas, S., Roberts, G., Schebeske, G., Sharma, S., Simo, R., Staubes, R., Turner, S. and Uher, G.,1999. A global database of sea surface dimethylsulfide (DMS) measurements and a procedure to predict sea surface DMS as a function of latitude, longitude and month. *Global Biogeochemical Cycles*, **13**, 399-444

Kristjánsson, J. E., Edwards, J. M. and Mitchell, D. L., 1999. A new parametrization scheme for the optical properties of ice crystals for use in general circulation models of the atmosphere. *Phys. and Chem. of the Earth*, **24**, 231-236

Langner, J. and Rodhe, H., 1991. A global three-dimensional model of the tropospheric sulfur cycle. *J. Atmos. Chem.*, **13**, 225-263

Lelieveld, J., Roelofs, G.-J., Ganzeveld, L., Feichter, J. and Rodhe, H., 1997. Terrestrial sources and distribution of atmospheric sulphur. *Phil. Trans. R. Soc. Lond. B*, **352**, 149-158.

Liss, P. S., Hatton, A. D., Malin, G., Nightingale, P. D. and Turner, S. M., 1997. Marine sulphur emissions. *Phil. Trans. R. Soc. Lond. B*, **352**, 159-169

Liss, P. S. and Merlivat, L., 1986. Air-sea gas exchange rates: introduction and synthesis. In: *The role of air-sea exchange in geochemical cycling* (ed. P. Buat-Menard). Reidel, Dordrecht

Lohmann, U. and Feichter, J., 1997. Impact of sulfate aerosols on albedo and lifetime of clouds: A sensitivity study with the ECHAM4 GCM. *J. Geophys. Res.*, **102**, 13685-13700

Martin, G. M., Johnson, D. W. and Spice, A., 1994. The measurement and parametrisation of effective radius of droplets in warm stratocumulus clouds. *J. Atmos. Sci.*, **51**, 1823-1842

Monteith, J. L. and Unsworth, M. H., 1990. *Principles of environmental physics (2nd edition)*, Edward Arnold, London

Murphy, D. M., Anderson, J. R., Quinn, P. K., McInness, L. M., Brechtel, F. J., Kreidenweis, S. M., Middlebrook, A. M., Pósfai, M., Thomson, D. S. and Buseck, P. R., 1998. Influence of sea-salt on aerosol radiative properties in the Southern Ocean marine boundary layer. *Nature*, **392**, 62-65

Noone, K. J., Russell, L. M., O'Dowd, C. D., Smith, M. H., Johnson, D. W., Hobbs, P. V., Flagan, R. C., Seinfeld, J. H., Durkee, P. A., Brooks, I. M., Rogers, D. and Garrett, T., 1999. A case study of ships forming and not forming tracks in a moderately polluted boundary layer. *J. Atmos. Sci.*, **56** (in press)

Noone, K. J., Öström, E., Pockalny, R. A., De Bock, L. and Van Grieken, R., 1996. Chemical and microphysical properties of cloud droplet residual particles in marine stratocumulus clouds observed during the MAST experiment. *Proc. 12th Int. Conf. on Clouds and Precipitation*, Zürich, 1176-1178

O'Dowd, C. D., Lowe, J. A. and Smith, M. H., 1999a. Coupling sea-salt and sulphate interactions and its impact on cloud droplet concentration predictions. *Geophys. Res. Let.*, **26**, 1311-1314

O'Dowd, C. D., Lowe, J. A. and Smith, M. H. and Kaye, A. D., 1999b. The relative importance of non-sea-salt sulphate and sea-salt aerosol to the marine cloud condensation nuclei population: An improved multi-component aerosol-cloud droplet parametrization. *Q. J. R. Meteorol. Soc.*, **125**, 1295-1313

O'Dowd, C. D., Smith, M. H., Consterdine, I. E. and Lowe, J. A., 1997. Marine aerosol, sea-salt, and the marine sulphur cycle: A short review. *Atmos. Environ.*, **31**, 73-80

O'Dowd, C. D. and Smith, M. H., 1993. Physicochemical properties of aerosol over the Northeast Atlantic: Evidence for wind-speed-related submicron sea-salt aerosol production. *J. Geophys. Res.*, **98**, 1137-1149

Pan, W., Tatang, M. A., McRae, G. J. and Prinn, R. G., 1998. Uncertainty analysis of indirect radiative forcing by anthropogenic sulfate aerosols. *J. Geophys. Res.*, **103**, 3815-3823

Penkett, S. A., Jones, B. M. R., Brice, K. A. and Eggleton, A. E. J., 1979. The importance of atmospheric ozone and hydrogen peroxide in oxidising sulphur dioxide in cloud and rainwater. *Atmos. Environ.*, **13**, 123-137

Pham, M., Müller, J.-F., Brasseur, G. P., Granier, C. and Mégie, G., 1995. A three-dimensional study of the tropospheric sulfur cycle. *J. Geophys. Res.*, **100**, 26061-26092

Pope, V. D., Gallani, M. L., Rowntree, P. R., and Stratton, R. A., 1999. The impact of new physical parametrizations in the Hadley Centre climate model — HadAM3. *Clim. Dyn.*(accepted)

Pruppacher, H. R. and Klett, J. D., 1997. *Microphysics of clouds and precipitation (2nd edition)*, Kluwer, Dordrecht

Quinn, P. K., Marshall, S. F., Bates, T. S., Covert, D. S. and Kapustin, V. N., 1995. Comparison of measured and calculated aerosol properties relevant to the direct radiative forcing of tropospheric sulfate aerosol on climate. *J. Geophys. Res.*, **100**, 8977-8991

Ravishankara, A. R., Rudich, Y., Talukdar, R., and Barone, S. B., 1997. Oxidation of atmospheric reduced sulphur compounds: perspective from laboratory studies. *Phil. Trans. Roy. Soc. B*, **352**, 171-182

Rivera-Carpio, C. A., Corrigan, C. E., Novakov, T., Penner, J. E., Rogers, C. F. and Chow, J. C., 1996. Derivation of contributions of sulfate and carbonaceous aerosols to cloud condensation nuclei from mass size distributions. *J. Geophys. Res.*, **101**, 19483-19493

Roe, P.L., 1985. Some contributions to the modelling of discontinuous flows. In: *Large-Scale Computations in Fluid Mechanics*, Lectures in Applied Mathematics **22**, 163-193. American Mathematical Society, Providence, Rhode Island

Roelofs, G.-J., Lelieveld, J. and Ganzeveld, L., 1998. Simulation of global sulfate distribution and the influence on effective cloud drop radii with a coupled photochemistry-sulfur cycle model. *Tellus B*, **50**, 224-242

Rogers, R. R. and Yau, M. K., 1989. *A short course in cloud physics (3rd. edition)*, Pergamon Press, Oxford

Rotstayn, L. D., 1999. Indirect forcing by anthropogenic aerosols: A global climate model calculation of the effective-radius and cloud-lifetime effects. *J. Geophys. Res.*, **104**, 9369-9380

Rutledge, S. A. and Hobbs, P. V., 1983. The mesoscale and microscale structure and organization of clouds and precipitation in mid-latitude cyclones. Part VII: A model for the "seeder-feeder" process in warm frontal rainbands. *J. Atmos. Sci.*, **40**, 1185-120

Seinfeld, J. H. and Pandis, S. N., 1998. *Atmospheric chemistry and physics: From air pollution to climate change*. John Wiley, New York

Smith, R. N. B., 1990. A scheme for predicting layer clouds and their water content in a general circulation model. *Q. J. R. Meteorol. Soc.*, **116**, 435-460

Snider, J. R. and Vali, G., 1994. Sulfur dioxide oxidation in winter orographic clouds. *J. Geophys. Res.*, **99**, 18713-18733

Spiro, P. A., Jacob, D. J. and Logan, J. A., 1992. Global inventory of sulfur emissions with 1^{o} x 1^{o} resolution. *J. Geophys. Res.*, **97**, 6023-6036

Stevenson, D. S., Collins, W. J., Johnson, C. E. and Derwent, R. G., 1997. The impact of aircraft nitrogen oxide emissions on tropospheric ozone studied with a 3D Lagrangian model including fully diurnal chemistry. *Atmos. Environ.*, **31**, 1837-1850

Tripoli, G. J. and Cotton, W. R., 1980. A numerical investigation of several factors contributing to the observed variable intensity of deep convection over South Florida. *J. App. Met.*, **19**, 1037-1063

Twomey, S. A., 1974. Pollution and the planetary albedo. *Atmos. Environ.*, **8**, 1251-1256

Twomey, S. A. 1977. *Atmospheric Aerosols (Developments in Atmospheric Science, Vol. 7)*, Elsevier, London

Wilson, D. R. and Ballard, S. P., 1999. A microphysically based precipitation scheme for the UK Meteorological Office Unified Model. *Q. J. R. Meteorol. Soc.*, **125**,1607-1636

Figure 1

(a) Annual-mean column-integrated SO_4^{2-} burden simulated using modern sulphur emissions (mg m^{-2}).

(b) As (a) but using pre-industrial emissions.

Figure 2

Comparison between modelled (top) and retrieved (bottom) cloud droplet effective radii (μm). The modelled distribution is from the modern-day simulation of experiment V (both indirect effects) and the satellite retrievals are from Han *et al.* (1994).

Figure 3

(a) Annual-mean change in TOA net radiation due to anthropogenic sulphate aerosols *via* the first indirect effect (Wm^{-2}). Negative values are indicated by solid contour lines, positive values by dashed contours.

(b) As (a) but for the second indirect effect.

(c) As (a) but for both indirect effects simultaneously.

Fig. 1

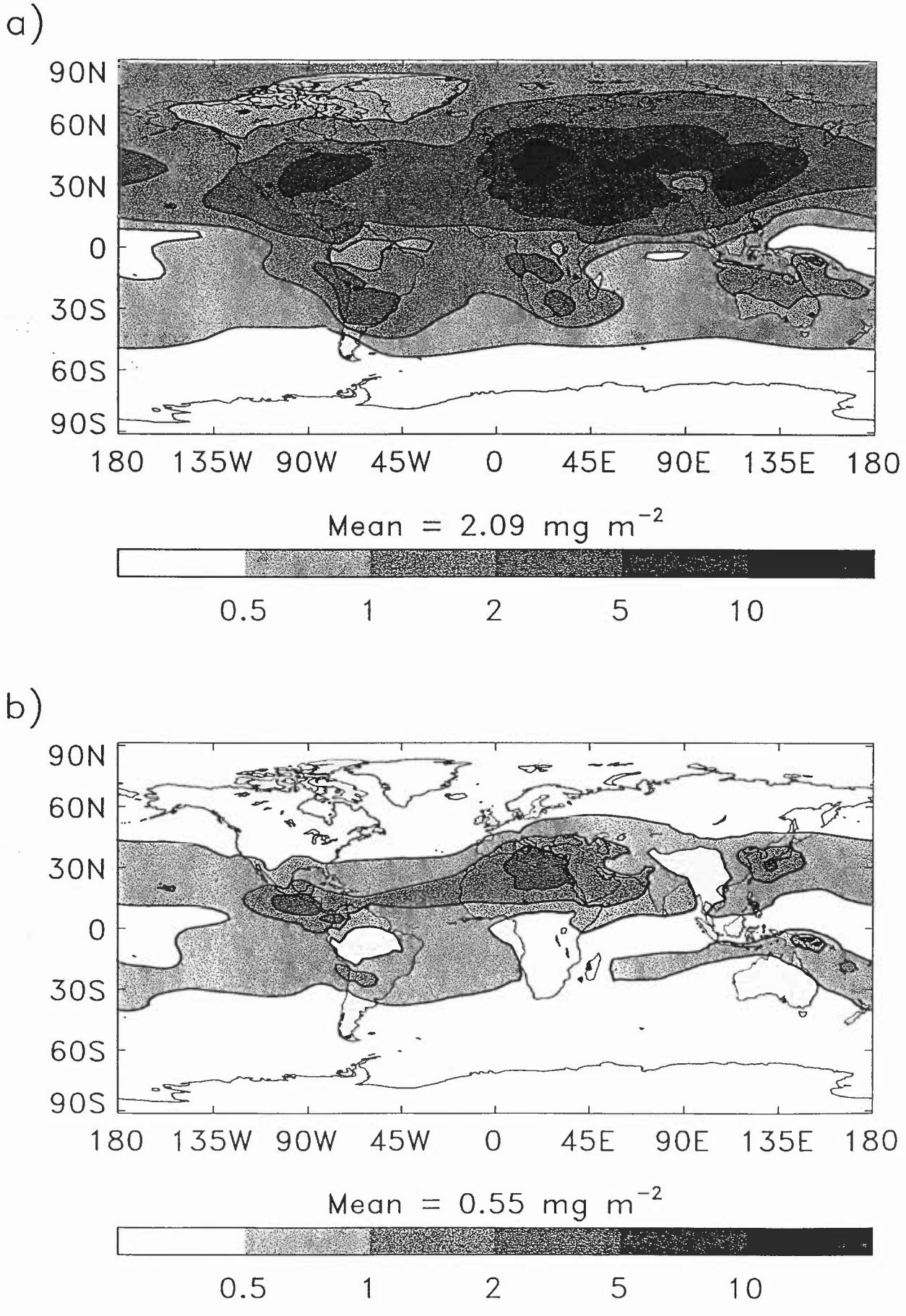
a)
90N
60N
30N
0
30S
60S
90S
180 135W 90W 45W 0 45E 90E 135E 180
Mean = 2.09 mg m^{-2}
0.5 1 2 5 10
b)
90N
60N
30N
0
30S
60S
90S
180 135W 90W 45W 0 45E 90E 135E 180
Mean = 0.55 mg m^{-2}
0.5 1 2 5 10

Fig. 2

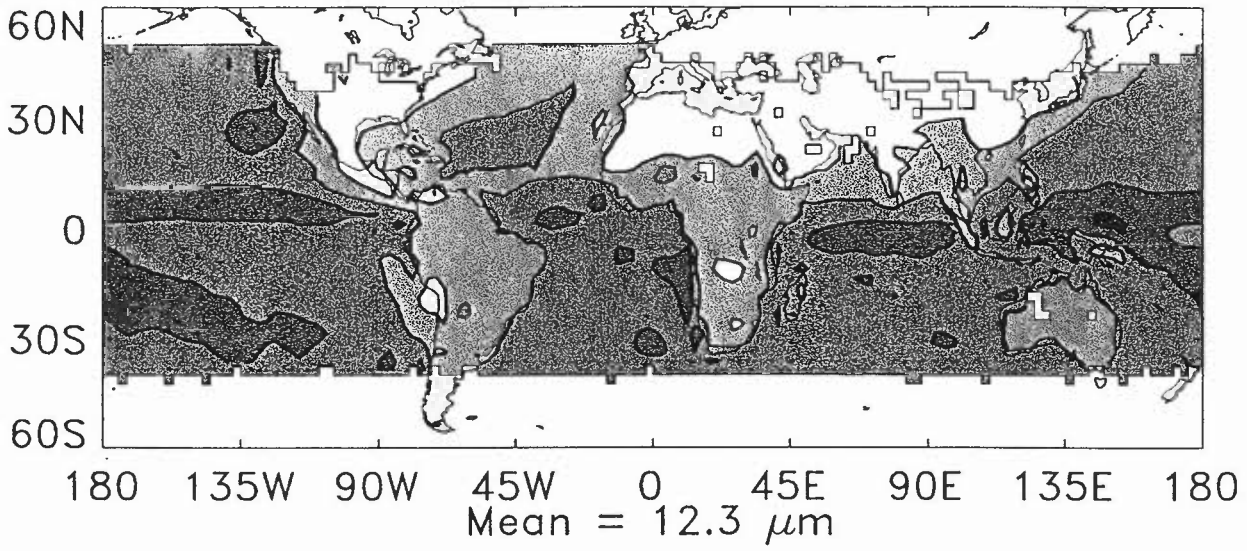
60N
30N
0
30S
60S
180 135W 90W 45W 0 45E 90E 135E 180
Mean = 12.3 μm

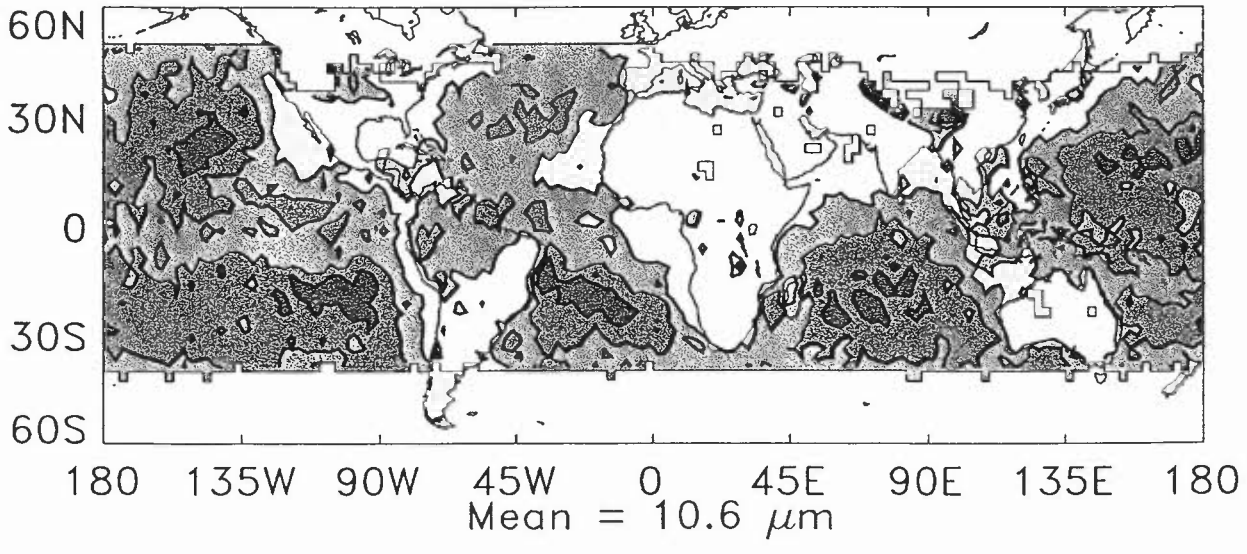
60N
30N
0
30S
60S
180 135W 90W 45W 0 45E 90E 135E 180
Mean = 10.6 μm


10
12
14
16

Fig. 3

a)

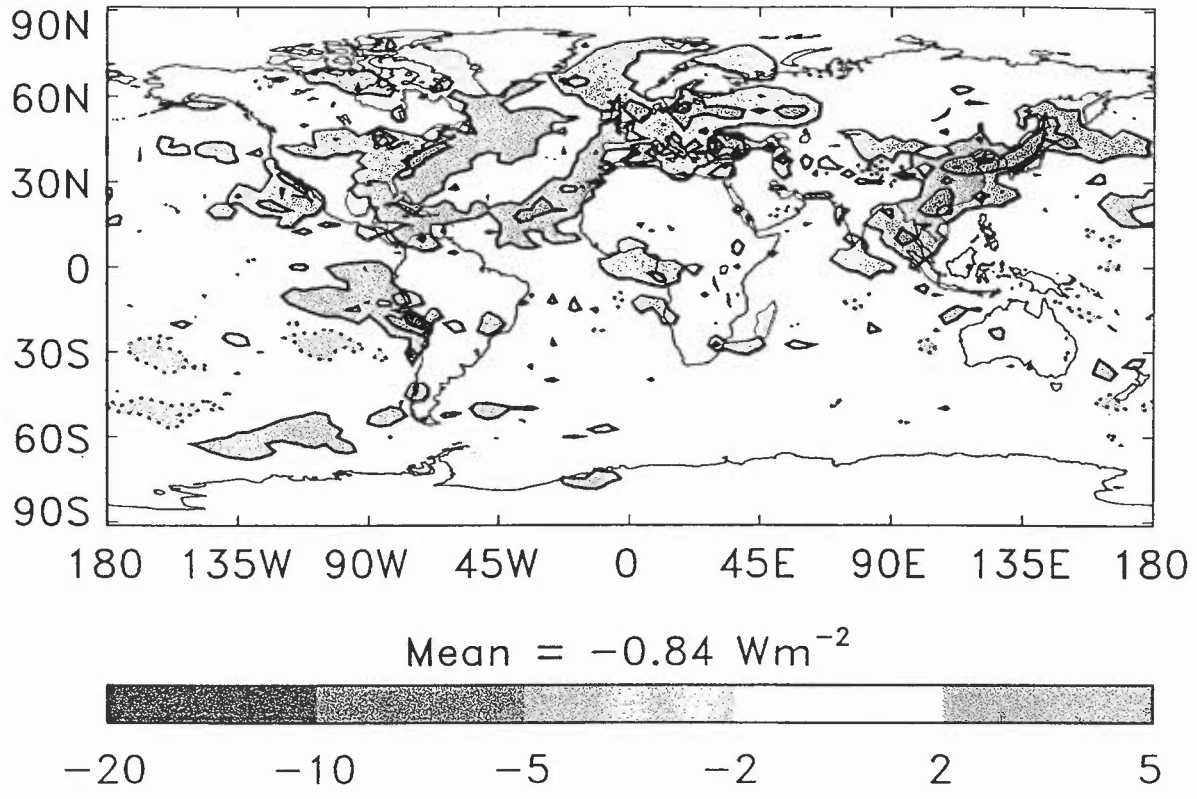
90N
60N
30N
0
30S
60S
90S
180 135W 90W 45W 0 45E 90E 135E 180
Mean = −0.84 Wm^{-2}
−20 −10 −5 −2 2 5

b)

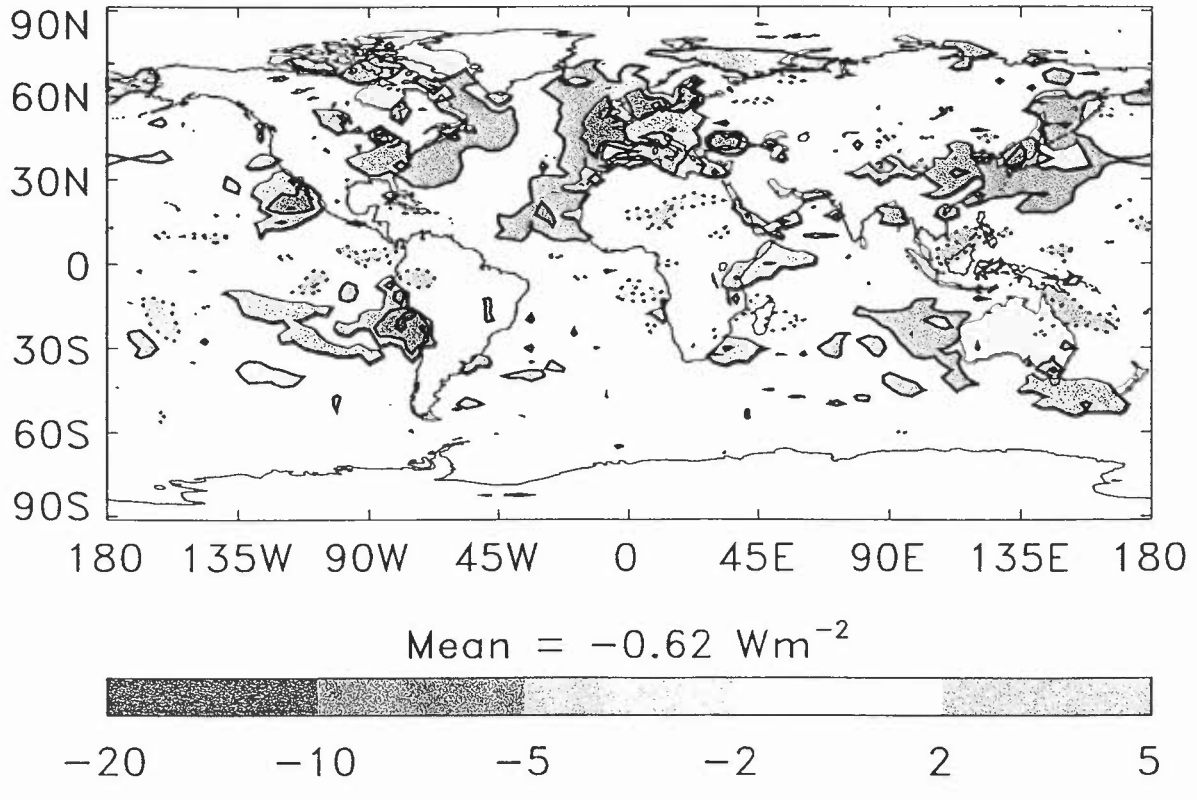
90N
60N
30N
0
30S
60S
90S
180 135W 90W 45W 0 45E 90E 135E 180
Mean = −0.62 Wm^{-2}
−20 −10 −5 −2 2 5

c)

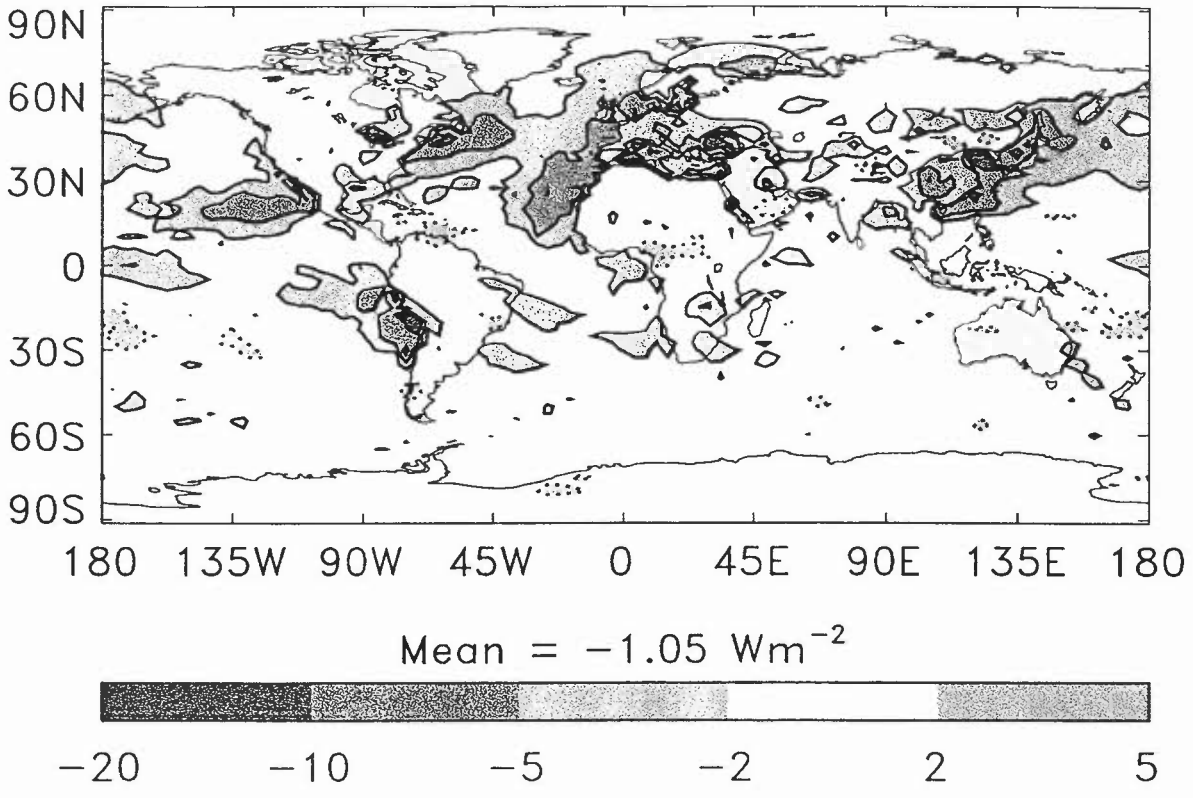
90N
60N
30N
0
30S
60S
90S
180 135W 90W 45W 0 45E 90E 135E 180
Mean = −1.05 Wm^{-2}
−20 −10 −5 −2 2 5